

Article

Energy Conversion Capacity of Barium Zirconate Titanate

Nawal Binhayeeniyi ^{1,*}, Pisan Sukwisute ² , Safitree Nawae ¹ and Nantakan Muensit ^{3,4}

¹ Faculty of Science and Technology, Princess of Naradhiwas University, Narathiwat 96000, Thailand; safitree.n@pnu.ac.th

² Department of Physics, Faculty of Science, King Mongkut's Institute of Technology Ladkrabang, Bangkok 10520, Thailand; pisan.su@kmitl.ac.th

³ Department of Physics, Faculty of Science, Prince of Songkla University, Songkhla 90110, Thailand; nantakan.m@psu.ac.th

⁴ Center of Excellence in Nanotechnology for Energy (CENE), Prince of Songkla University, Songkhla 90110, Thailand

* Correspondence: nawal.b@pnu.ac.th

Received: 6 November 2019; Accepted: 7 January 2020; Published: 9 January 2020



Abstract: In this study, we investigated the effect of zirconium content on lead-free barium zirconate titanate (BZT) ($\text{Ba}(\text{Zr}_x\text{Ti}_{1-x})\text{O}_3$, with $x = 0.00, 0.01, 0.03, 0.05,$ and 0.08), which was prepared by the sol–gel method. A single-phase perovskite BZT was obtained under calcination and sintering conditions at $1100\text{ }^\circ\text{C}$ and $1300\text{ }^\circ\text{C}$. Ferroelectric measurements revealed that the Curie temperature of BaTiO_3 was 399 K , and the transition temperature decreased with increasing zirconium content. At the Curie temperature, $\text{Ba}(\text{Zr}_{0.03}\text{Ti}_{0.97})\text{O}_3$ with a dielectric constant of $19,600$ showed the best performance in converting supplied mechanical vibration into electrical power. The experiments focused on piezoelectric activity at a low vibrating frequency, and the output power that dissipated from the BZT system at 15 Hz was 2.47 nW ($30\text{ M}\Omega$). The prepared lead-free sol–gel BZT is promising for energy-harvesting applications considering that the normal frequencies of ambient vibration sources are less than 100 Hz .

Keywords: lead-free ceramic; sol–gel process; barium zirconate titanate; dielectric property

1. Introduction

Lead zirconate titanate (PZT, $\text{Pb}(\text{Zr}_x\text{Ti}_{1-x})\text{O}_3$), a lead-based material with a high piezoelectric coefficient and electromechanical coupling factor, is one of the most promising materials for use in fabricated energy-harvesting devices [1–3] because its perovskite structure exhibits dielectric, ferroelectric, and piezoelectric properties [2,3]. However, PZT is toxic to the environment. Therefore, innovative lead-free dielectric materials with piezoelectric properties have been formulated to address this environmental issue. Among these materials is BaTiO_3 , which is a well-known material possessing a perovskite structure with high dielectric properties, a low dielectric loss tangent, and dielectric reliability [4–7].

BaTiO_3 can be modified by doping it with additives such as Sr^{2+} , Ca^{2+} , Sn^{4+} , and Zr^{4+} [4]. Doping BaTiO_3 with ZrO_2 can improve the dielectric and piezoelectric properties because the chemical stability of Zr^{4+} is greater than that of Ti^{4+} [4–7]. In addition, the Curie temperature also changes; that is, it decreases as the Zr content increases [5–8].

BaTiO_3 can be used in tunable capacitor devices and dynamic random-access memory applications. Moreover, it is also applied in actuators and energy storage devices because the strain that is induced by the electric field retains dipole moment behavior and energy storage properties [7,9,10]. Lui et al.

prepared BaTi_{0.7}Zr_{0.3}O₃ ceramic by spark plasma sintering. The maximum energy storage density of the ceramic was determined to be 0.51 J/cm³ [9]. Moreover, Puli et al. investigated the energy storage of barium calcium titanate (BCT) ceramic and obtained a high energy density (0.24 J/cm³) [10].

There are various kinds of energy harvesters, including thermoelectric, electromagnetic, electrostatic, and piezoelectric. Of these methods, piezoelectric energy harvesting is very attractive for the system's small size, high output power, and ease of operation [11–13].

In this study, we investigated the crystal structure, dielectric properties, phase transition, and the degree of diffuseness of lead-free barium zirconate titanate (BZT) ceramics with various Zr contents. Additionally, the energy conversion behavior resulting from the modification of BZT was examined. These materials might lead to a reduction in the use of the lead-based bulky ceramics that are usually required in applications.

2. Materials and Methods

Ba(Zr_xTi_{1-x})O₃ ($x = 0.00, 0.01, 0.03, 0.05, \text{ and } 0.08$) was prepared by the sol–gel method. Barium acetate (HIMEDIA[®], Mumbai, MH, India, 99.0%), zirconium(IV) propoxide (Sigma-Aldrich[®], St. Louis, MO, USA, 70 wt.% in 1-propanol), and titanium(IV) isopropoxide (Sigma-Aldrich[®], St. Louis, MO, USA), were used as the reagents. Glacial acetic acid (Merck, Darmstadt, HE, Germany, 100%) and 2-methoxyethanol (Ajex Finechem Pty Ltd, Taren Point, NSW, Australia) were used as solvents in the sol–gel method following Jiwei et al. [14]. The procedure has been reported elsewhere [15,16]. The gels were dried in an oven for 24 h. All dried gels were calcined at 1100 °C for 2 h in alumina crucibles. The BZT powder was ball-milled in ethanol milling media (Merck, Ethanol Absolute, Darmstadt, HE, Germany) for 24 h (200 rpm) by using a high-energy planetary ball mill (Retsch PM100, Haan, NW, Germany). The milled powders were blended with a small amount of polyvinyl alcohol (PVA) to form discs (diameter 13 mm) at 100 MPa. All the green bodies were sintered at 1300 °C for 2 h in closed alumina crucibles. The upper and lower surfaces of the sintered ceramics were covered by silver paste and then calcined at 600 °C for 0.5 h for use as electrodes for the dielectric measurements.

The dielectric properties and ferroelectric phase transitions of all samples were characterized at 25–150 °C (at 1 kHz) by an LCR meter (Hewlett Packard 4263 B, Mississauga, ON, Canada). The crystalline structure of BZT was determined by X-ray diffraction (XRD, PHILLIPS X'pert MPD, Almelo, OV, Netherlands) with Ni-filtered CuK_α radiation. The XRD analysis was performed at room temperature ($20^\circ \leq 2\theta \leq 77^\circ$) with a step size of 0.02°. The bulk densities of the sintered BZT discs were measured in accordance with the Archimedes method. Thermal analysis of the dried BZT gels was performed by differential thermal analysis (DTA, Perkin Elmer DTA7, Norwalk, CT, USA) and thermogravimetric analysis (TGA, Perkin Elmer TGA7, Norwalk, CT, USA). The thermal analysis results were collected from 50 °C to 1300 °C at a rate of 10° C/min. Surface microstructures were observed using scanning electron microscopy (SEM, quanta400, Thermo Fisher Scientific, Brno, JM, Czech Republic) with an accelerating voltage of 20 kV and 3000× magnification. The grain sizes were analyzed by averaging over the total number of grains in the SEM images.

3. Results and Discussion

The TGA and DTA results in Figure 1 show three mechanisms. First, the endothermic reaction observed in the temperature range of 25–200 °C is associated with the dehydration of the dried BZT gels, as observed by the mass loss of about 20%. Second, in the temperature range of 200–650 °C, a major mass loss occurs with the emission of CO₂, solvents, and organic compounds because of the thermal disintegration of the polymeric dried gels and primary synthesis of Ba(Zr_xTi_{1-x})O₃ via BaCO₃–TiO₂ and BaCO₃–ZrO₂ core–shell particles [17–19]. Third, the exothermic peak in the range of 650–1200 °C exhibits a slight weight loss that can be attributed to Ba(Zr_xTi_{1-x})O₃ crystallization and the subsequent formation of the perovskite structure. This final mechanism is due to the decarbonation of BaCO₃ to react with TiO₂ and ZrO₂. For these results, it is worth noting that although the calcination process is typically performed at temperatures as low as 650 °C, the calcination temperature used in this work

was 1100 °C [15,16] to ensure the formation of the pure perovskite structure of $\text{Ba}(\text{Zr}_x\text{Ti}_{1-x})\text{O}_3$ without secondary phases, as seen in the following XRD result (Figure 2). Calcination at a temperature above 1100 °C should not be undertaken, because of the agglomeration and enlargement of $\text{Ba}(\text{Zr}_x\text{Ti}_{1-x})\text{O}_3$ particles. The compression of large calcined particles might result in a low bulk density of the sintered ceramics [20,21]. Table 1 presents the measurable bulk density of sintered $\text{Ba}(\text{Zr}_x\text{Ti}_{1-x})\text{O}_3$. The relative density of all samples is $93.5\% \pm 0.21\%$. The addition of zirconium does not affect density [8]. A sintering temperature of 1300 °C is sufficient to fuse the as-calcined $\text{Ba}(\text{Zr}_x\text{Ti}_{1-x})\text{O}_3$ powders, and a calcination temperature of 1100 °C has an insignificant effect on the bulk density. The XRD patterns of sintered $\text{Ba}(\text{Zr}_x\text{Ti}_{1-x})\text{O}_3$ ceramics (with $x = 0.00, 0.01, 0.03, 0.05,$ and 0.08) are shown in Figure 2. The structure of all $\text{Ba}(\text{Zr}_x\text{Ti}_{1-x})\text{O}_3$ ceramics is a pure perovskite phase without an impurity phase. With the addition of Zr, the peak shifts to a lower angle because the ionic radius of Zr^{4+} (0.079 nm) is larger than that of Ti^{4+} (0.068 nm) [5]. It is clear that the tetragonal phase of BaTiO_3 ceramic is characterized by the splitting of the (0 0 2) and (2 0 0) diffraction peaks at 44.93° and 45.40° , respectively (the calculated values of the cell parameters of BaTiO_3 are ($a \sim 3.9906 \text{ \AA}$, $c \sim 4.0301 \text{ \AA}$), respectively). As the zirconium content increases, the two diffraction peaks merge into one peak. This corresponds with the change in the structure of the BZT system from tetragonal to orthorhombic at room temperature, as previously reported by [4,6,22]. According to, the separation of (1 3 3) and (3 1 1) diffraction peaks of $\text{Ba}(\text{Zr}_{0.03}\text{Ti}_{0.07})\text{O}_3$ occurs at diffraction angles of 74.63° and 74.91° , respectively; upon the addition of 5 mol.% zirconium content, a single diffraction peak is observed. This is caused by the structure transforming from orthorhombic to rhombohedral [4,6]. It is concluded that the increased zirconium content changes the structure of BZT ceramic from tetragonal to rhombohedral, which is confirmed by the gradual merging of XRD peaks [6,8,21]. Finally, the dense ceramic discs exhibit large grains and a small proportion of fine grains with pores. The grains are irregular in shape, with an average grain size of 10–30 μm , because the initial size of the powder is changed by the ball milling process [20,21], as shown in Figure 3.

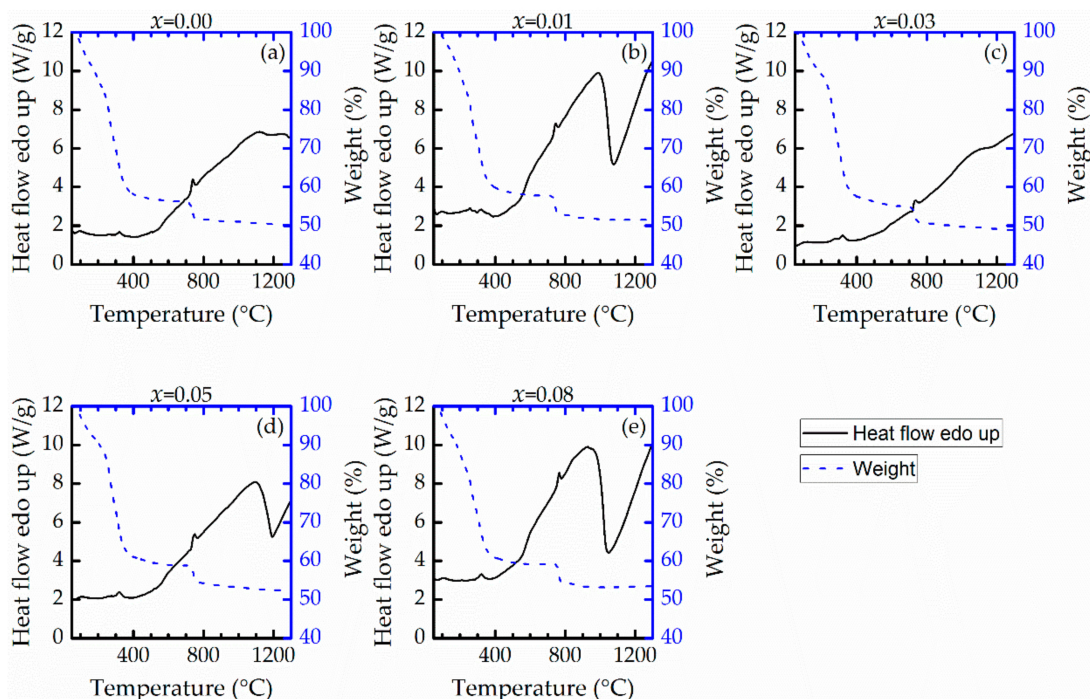


Figure 1. TGA and DTA plots for $\text{Ba}(\text{Zr}_x\text{Ti}_{1-x})\text{O}_3$ samples with x composition of (a) 0.00, (b) 0.01, (c) 0.03, (d) 0.05 and (e) 0.08 mol.

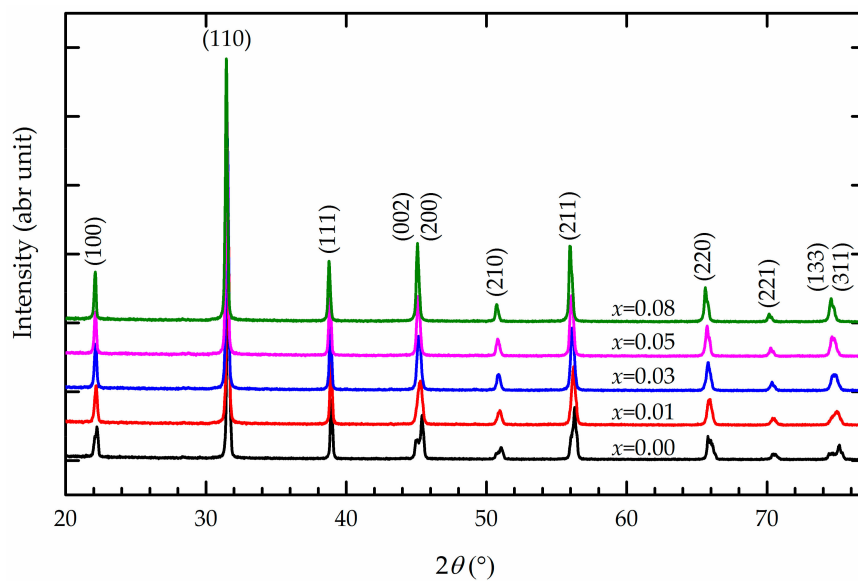


Figure 2. XRD patterns of the $\text{Ba}(\text{Zr}_x\text{Ti}_{1-x})\text{O}_3$ ceramics.

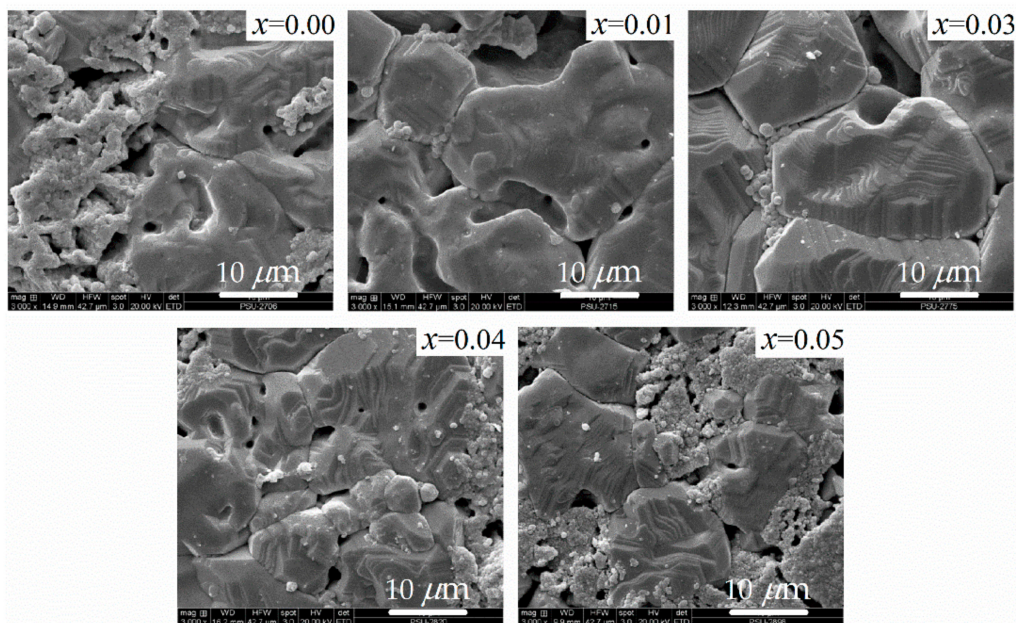


Figure 3. SEM images of the sintered $\text{Ba}(\text{Zr}_x\text{Ti}_{1-x})\text{O}_3$ ceramics.

Table 1. Relative density, the values of the dielectric constant (ϵ_r) at T_m (1 kHz), dielectric loss ($\tan\delta$) at T_m (1 kHz), Curie–Weiss temperature (T_0), Curie–Weiss constant (C), Curie–Weiss law temperature (T_{cw}), T_m , ΔT_m , and γ for all x values of $\text{Ba}(\text{Zr}_x\text{Ti}_{1-x})\text{O}_3$.

$\text{Ba}(\text{Zr}_x\text{Ti}_{1-x})\text{O}_3$	Relative Density (%)	ϵ_r at T_m (1 kHz)	$\tan\delta$ at T_m (1 kHz)	T_0 (K)	C ($\times 10^5$ K)	T_{cw} (K)	T_m (K)	ΔT_m (K)	γ
$x = 0.00$	93.26	9,496	0.0072	357	4.04	400	399	1	1.01
$x = 0.01$	93.66	15,702	0.0207	366	4.08	395	392	3	1.05
$x = 0.03$	93.76	19,698	0.0314	353	3.92	378	370	8	1.21
$x = 0.05$	93.49	16,891	0.0382	335	3.79	368	353	14	1.26
$x = 0.08$	93.32	11,294	0.0392	312	3.36	355	331	24	1.38

The relative permittivity (ϵ_r) or dielectric constant and dielectric loss ($\tan\delta$) at T_m (1 kHz) are listed in Table 1. The dielectric constant increases with zirconium content until it reaches 3 mol.%. $\text{Ba}(\text{Zr}_{0.03}\text{Ti}_{0.97})\text{O}_3$ ceramic has the highest dielectric constant, which is reduced when zirconium reaches

5 mol.%. The dielectric loss of all BZT ceramics depends on the zirconium content and ranges from 0.072 to 0.0392, similar to the results of our previous work [15].

Figure 4 presents the values of the relative permittivity (ϵ_r) or dielectric constant measured at 1 kHz for the $\text{Ba}(\text{Zr}_x\text{Ti}_{1-x})\text{O}_3$ samples. The position of each dielectric peak moves to a higher temperature with the addition of Zr, which ranges from 0 to 3 mol.%. For $x = 0.08$, the dielectric peak is broad because of the inhomogeneous distribution of Zr^{4+} ions in the Ti sites and the non-uniform stress in the grains [8,23]. The highest dielectric constant is 19,600 for $\text{Ba}(\text{Zr}_{0.03}\text{Ti}_{0.97})\text{O}_3$. Further increases in Zr content cause a decrease in the temperature T_m with the maximum dielectric value (Table 1), as described in the literature [6,8]. This is the result of the increased substitution of the Zr^{4+} ion in the B sites of BaTiO_3 , causing a change in the d -spacing of the $\text{Ba}(\text{Zr}_x\text{Ti}_{1-x})\text{O}_3$ structure [6,16] and resulting in a decrease in the phase transition temperature or T_m [8,22]. For low Zr content ($x < 0.15$), at the apex of the dielectric curve, T_m can be considered the Curie temperature (T_c) [21]. A rapid increase in the ϵ_r value occurs near T_c because the BZT structure is thermally excited to a tetragonal–cubic intermediate phase (ferroelectric–paraelectric phase transition) when the temperature changes to T_m . This results in a large degree of unstable polarization, and consequently, an applied electric field can easily produce considerable variation in polarization [24]. The decrease in the dielectric constant above T_c is caused by the thermal detriment of polarization alignment [24,25].

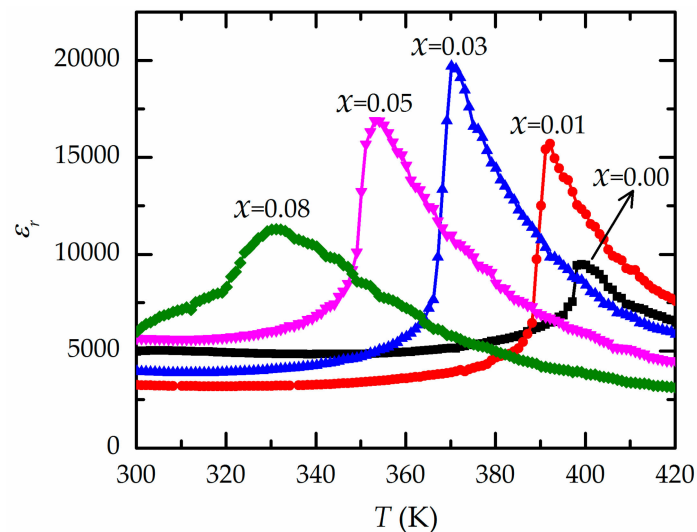


Figure 4. Relationships between the dielectric constant (ϵ_r) and temperature for all samples of $\text{Ba}(\text{Zr}_x\text{Ti}_{1-x})\text{O}_3$ ceramics.

Because BZT ceramic is classified as a ferroelectric material, the dielectric characteristic of BZT above the Curie temperature corresponds to the Curie–Weiss law: $1/\epsilon_r = (T - T_0)/C$ ($T > T_c$), where T_0 and C are the Curie–Weiss temperature and constant, respectively. For all analyzed BZT compositions, the inverse ϵ_r versus temperature data were fitted to the Curie–Weiss law, as shown in Figure 5. The T_0 fitting parameters are listed in Table 1. It is clear that the reciprocal ϵ_r value follows the Curie–Weiss law for $T > T_m$. The divergence of the reciprocal ϵ_r value from the Curie–Weiss law is defined as $\Delta T_m = T_{cw} - T_m$, where T_{cw} is the temperature at which the value of the reciprocal ϵ_r value begins to diverge from the Curie–Weiss law. From the results in Table 1, the ΔT_m value increases with Zr content because of the influence of the Zr^{4+} ions on the shift in the ferroelectric–paraelectric transition temperature of BZT [5,6,26].

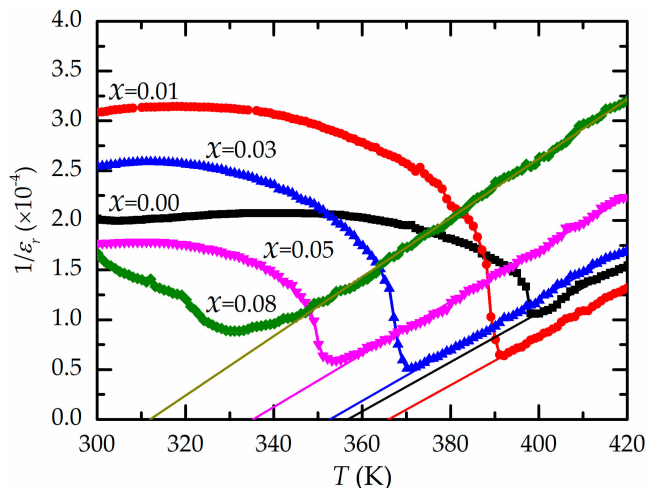


Figure 5. Relationships between the temperature and the inverse dielectric constant at 1 kHz for all the Ba(Zr_xTi_{1-x})O₃ ceramics.

The degree of diffuseness of the phase transition can be formulated by a modified Curie–Weiss law [27]:

$$\frac{1}{\epsilon_r} - \frac{1}{\epsilon_m} = \frac{(T - T_m)^\gamma}{C^*} \quad (1 \leq \gamma \leq 2), \tag{1}$$

where γ and C^* are constants derived from fitting the experimental data. The γ value provides information about the behavior of ferroelectric materials. For a normal ferroelectric, $\gamma = 1$. For an ideal ferroelectric relaxor associated with quadratic dependence, $\gamma = 2$. Figure 6 shows the plot of $\ln(1/\epsilon_r - 1/\epsilon_m)$ against $\ln(T - T_m)$ at 1 kHz. The fitted γ values (Table 1) show that the higher the Zr content, the higher the diffuse phase transition, as reported in previous works [6,8]. Consequently, the inclusion of the diffusive Zr⁴⁺ ion in the octahedral site of the perovskite structure causes the common ferroelectric to transform into a ferroelectric relaxor [9,28]. The dielectric losses of all the BZT ceramics range from 1% to 5%. It is clear that the dielectric losses show the same trends with increasing temperature.

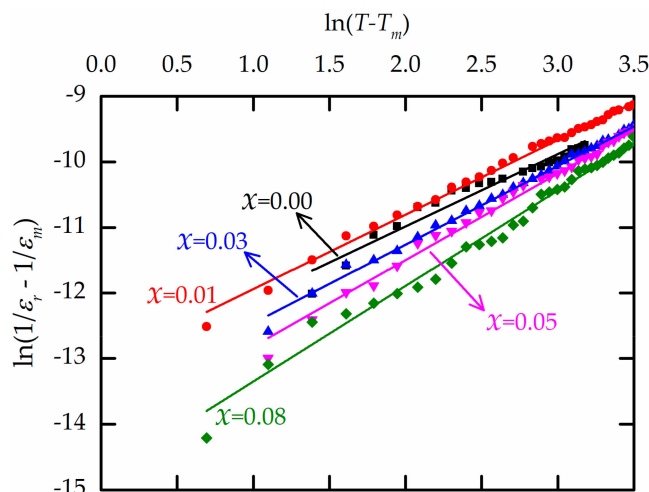


Figure 6. Linear relationships between $\ln(1/\epsilon_r - 1/\epsilon_m)$ and $\ln(T - T_m)$ for all x values.

Each sample was investigated for the capability of energy conversion, as described by Sukwisute et al. [1]. Each disc (thickness ~ 1 mm) was rigidly glued onto a vibrating structure at a constant operating frequency of 15 Hz. Varying resistors were connected to each disc, and the potential in the circuit was measured to calculate the output power according to $P_{ac} = V^2/R$, where V is the potential

and R is the resistance. The calculated values are summarized in Table 2. The $\text{Ba}(\text{Zr}_{0.03}\text{Ti}_{0.97})\text{O}_3$ ceramic shows the capability of energy conversion of the supplied mechanical vibration to electrical power. This is attributed to the highest dielectric constants and the transformation of the common ferroelectric to a relaxor ferroelectric, as reported previously [9,28]. In previous work, Rukbamrung et al. used the standard harvesting approach to determine the energy-harvesting ability of PZT + 1 mol.% Mn and PMN-25PT, and they obtained a power of 1.7 and 4.5 μW [2]. The BZT ceramics in our study can be operated at the low frequencies used in daily activities, such as walking and running. In addition, the normal frequencies of ambient vibration sources are much less than 100 Hz [11,12]. From this practical viewpoint, BZT ceramic can be very useful in low-frequency energy-harvesting devices.

Table 2. Output power dissipated from the barium zirconate titanate (BZT) system.

$\text{Ba}(\text{Zr}_x\text{Ti}_{1-x})\text{O}_3$	V (± 0.05 V)	R (M Ω)	P _{ac} (nW)
$x = 0.00$	0.24	132	0.044
$x = 0.01$	0.26	90	0.075
$x = 0.03$	0.86	30	2.47
$x = 0.05$	0.68	50	0.92
$x = 0.08$	0.28	90	0.09

4. Conclusions

$\text{Ba}(\text{Zr}_x\text{Ti}_{1-x})\text{O}_3$ ceramics with various zirconium contents ($x = 0.00, 0.01, 0.03, 0.05,$ and 0.08) were produced by the sol–gel method. A single-phase perovskite BZT was obtained under calcination and sintering conditions at 1100 °C and 1300 °C. All BZT samples had a pure perovskite structure without a secondary phase. The crystal structure changed with the zirconium content. Ferroelectric measurements of the ceramics showed that the Curie temperature of BaTiO_3 was 399 K, and further increases in the zirconium content decreased the Curie temperature to 331 K. At the phase transition, $\text{Ba}(\text{Zr}_{0.03}\text{Ti}_{0.97})\text{O}_3$ had the highest dielectric constant of 19,600 and exhibited good performance in converting supplied mechanical vibration to electrical power. Thus, $\text{Ba}(\text{Zr}_{0.03}\text{Ti}_{0.97})\text{O}_3$ is promising for mechanical energy-to-electrical energy coupling at low frequencies, with no damage observed at high temperatures.

Author Contributions: N.B. performed the experiments, characterization, data analysis, research discussion and manuscript preparation. P.S. and N.M. provided the supervision and research discussion. N.B., P.S., N.M. and S.N. reviewed the manuscript. All authors have read and agreed to the published version of the manuscript.

Funding: This research was supported by the Faculty of Science and Technology, Princess of Naradhiwas University, Thailand.

Acknowledgments: The authors are profoundly grateful to the Faculty of Science and Technology, Princess of Naradhiwas University, the Faculty of Science, King Mongkut’s Institute of Technology Ladkrabang, and the Department of Physics and the Center of Excellence in Nanotechnology for Energy at the Prince of Songkla University for equipment and other support.

Conflicts of Interest: The authors declare no conflict of interest.

References

- Sukwisute, P.; Muensit, N.; Soontaranon, S.; Rugmai, S. Micropower energy harvesting using poly (vinylidene fluoride hexafluoropropylene). *Appl. Phys. Lett.* **2013**, *103*, 063905. [[CrossRef](#)]
- Rakbamrung, P.; Lallart, M.; Guyomar, D.; Muensit, N.; Thanachayanont, C.; Lucat, C.; Guiffard, B.; Petit, L.; Sukwisut, P. Performance comparison of PZT and PMN-PT piezoceramics for vibration energy harvesting using standard or nonlinear approach. *Sens. Actuators A Phys.* **2010**, *163*, 493–500. [[CrossRef](#)]

3. Lü, C.; Zhang, Y.; Zhang, H.; Zhang, Z.; Shen, M.; Chen, Y. Generalized optimization method for energy conversion and storage efficiency of nanoscale flexible piezoelectric energy harvesters. *Energy Convers. Manag.* **2019**, *182*, 34–40.
4. Acosta, M.; Novak, N.; Rojas, V.; Patel, S.; Vaish, R.; Koruza, J.; Rossetti, G.A.; Rödel, J. BaTiO₃-based piezoelectrics: Fundamentals, current status, and perspectives. *Appl. Phys. Rev.* **2017**, *4*, 041305. [[CrossRef](#)]
5. Shen, B.; Zhang, Q.; Zhai, J.; Xu, Z. DC field effect on dielectric property of Ba (Zr_xTi_{1-x}) O₃ ceramics. *Ceram. Int.* **2013**, *39*, S9–S13. [[CrossRef](#)]
6. Kuang, S.J.; Tang, X.G.; Li, L.Y.; Jiang, Y.P.; Liu, Q.X. Influence of Zr dopant on the dielectric properties and Curie temperatures of Ba(Zr_xTi_{1-x})O₃ (0 ≤ x ≤ 0.12) ceramics. *Scr. Mater.* **2009**, *61*, 68–71. [[CrossRef](#)]
7. Yang, L.; Kong, X.; Li, F.; Hao, H.; Cheng, Z.; Liu, H.; Li, J.-F.; Zhang, S. Perovskite lead-free dielectrics for energy storage applications. *Prog. Mater. Sci.* **2019**, *102*, 72–108. [[CrossRef](#)]
8. Julphunthong, P.; Chootin, S.; Bongkarn, T. Phase formation and electrical properties of Ba (Zr_xTi_{1-x}) O₃ ceramics synthesized through a novel combustion technique. *Ceram. Int.* **2013**, *39*, S415–S419. [[CrossRef](#)]
9. Liu, B.; Wu, Y.; Huang, Y.H.; Song, K.X.; Wu, Y.J. Enhanced dielectric strength and energy storage density in BaTi_{0.7}Zr_{0.3} O₃ ceramics via spark plasma sintering. *J. Mater. Sci.* **2019**, *54*, 4511–4517. [[CrossRef](#)]
10. Puli, V.S.; Pradhan, D.K.; Riggs, B.C.; Chrisey, D.B.; Katiyar, R.S. Investigations on structure, ferroelectric, piezoelectric and energy storage properties of barium calcium titanate (BCT) ceramics. *J. Alloys Compd.* **2014**, *584*, 369–373. [[CrossRef](#)]
11. Dhakar, L.; Liu, H.; Tay, F.E.H.; Lee, C. A new energy harvester design for high power output at low frequencies. *Sens. Actuators A Phys.* **2013**, *199*, 344–352. [[CrossRef](#)]
12. Selvan, K.V.; Muhammad, M.S. Micro-scale energy harvesting devices: Review of methodological performances in the last decade. *Renew. Sust. Energ. Rev.* **2016**, *54*, 1035–1047. [[CrossRef](#)]
13. Zhang, X.; Gao, S.; Li, D.; Jin, L.; Wu, Q.; Liu, F. Frequency up-converted piezoelectric energy harvester for ultralow-frequency and ultrawide-frequency-range operation. *Appl. Phys. Lett.* **2018**, *112*, 163902. [[CrossRef](#)]
14. Jiwei, Z.; Xi, Y.; Liangying, Z.; Bo, S.; Chen, H. Orientation control and dielectric properties of sol-gel deposited Ba(Ti, Zr)O₃ thin films. *J. Cryst. Growth* **2004**, *262*, 341–347. [[CrossRef](#)]
15. Binhayeeniyi, N.; Sukvisut, P.; Thanachayanont, C.; Muensit, S. Physical and electromechanical properties of barium zirconium titanate synthesized at low-sintering temperature. *Mater. Lett.* **2010**, *64*, 305–308. [[CrossRef](#)]
16. Thanachayanont, C.; Yordsri, V.; Kijamnajsuk, S.; Binhayeeniyi, N.; Muensit, N. Microstructural investigation of sol-gel BZT powders. *Mater. Lett.* **2012**, *82*, 205–207. [[CrossRef](#)]
17. Wang, Z.; Zhao, K.; Guo, X.; Sun, W.; Jiang, H.; Han, X.; Tao, X.; Cheng, Z.; Zhao, H.; Kimura, H.; et al. Crystallization, phase evolution and ferroelectric properties of sol-gel-synthesized Ba(Ti_{0.8}Zr_{0.2})O_{3-x}(Ba_{0.7}Ca_{0.3})TiO₃ thin films. *J. Mater. Chem. C* **2013**, *1*, 522–530. [[CrossRef](#)]
18. Buscaglia, M.T.; Buscaglia, V.; Alessio, R. Coating of BaCO₃ crystals with TiO₂: Versatile approach to the synthesis of BaTiO₃ tetragonal nanoparticles. *Chem. Mater.* **2007**, *19*, 711–718. [[CrossRef](#)]
19. Mochizuki, Y.; Tsubouchi, N.; Sugawara, K. Synthesis of BaTiO₃ nanoparticles from TiO₂-coated BaCO₃ particles derived using a wet-chemical method. *J. Asian Ceram. Soc.* **2014**, *2*, 68–76. [[CrossRef](#)]
20. Maiwa, H. Electromechanical properties of Ba (Zr_{0.2}Ti_{0.8}) O₃ ceramics prepared by spark plasma sintering. *Ceram. Int.* **2012**, *38*, S219–S223. [[CrossRef](#)]
21. Xu, Q.; Zhan, D.; Huang, D.P.; Liu, H.X.; Chen, W.; Zhang, F. Dielectric inspection of BaZr_{0.2}Ti_{0.8}O₃ ceramics under bias electric field: A survey of polar nano-regions. *Mater. Res. Bull.* **2012**, *47*, 1674–1679. [[CrossRef](#)]
22. Hemedat, O.M.; Salem, B.I.; Abdelfatah, H.; Abdelsatar, G.; Shihab, M. Dielectric and ferroelectric properties of barium zirconate titanate ceramics prepared by ceramic method. *Phys. B* **2019**, *574*, 411680. [[CrossRef](#)]
23. Tang, X.G.; Wang, J.; Wang, X.X.; Chan, H.L.W. Effects of grain size on the dielectric properties and tunabilities of sol-gel derived Ba (Zr_{0.2}Ti_{0.8}) O₃ ceramics. *Solid State Commun.* **2004**, *131*, 163–168. [[CrossRef](#)]
24. Xue, D.; Gao, J.; Zhou, Y.; Ding, X.; Sun, J.; Lookman, T.; Ren, X. Phase transitions and phase diagram of Ba(Zr_{0.2}Ti_{0.8})O_{3-x}(Ba_{0.7}Ca_{0.3})TiO₃ Pb-free system by anelastic measurement. *J. Appl. Phys.* **2015**, *117*, 124107. [[CrossRef](#)]
25. Trainer, M. Ferroelectrics and the Curie-Weiss law. *Eur. J. Phys.* **2000**, *21*, 459–464. [[CrossRef](#)]
26. Sun, Z.; Li, L.; Zheng, H.; Yu, S.; Xu, D. Effects of sintering temperature on the microstructure and dielectric properties of BaZr_{0.2}Ti_{0.8}O₃ ceramics. *Ceram. Int.* **2015**, *41*, 12158–12163. [[CrossRef](#)]

27. Uchino, K.; Nomura, S. Critical exponents of the dielectric constants in diffused-phase-transition crystals. *Ferroelectr. Lett. Sect.* **1982**, *44*, 55–61. [[CrossRef](#)]
28. Ahmad, M.M.; Alismail, L.; Alshoaibi, A.; Aljaafari, A.; Kotb, H.M.; Hassanien, R. Dielectric behavior of spark plasma sintered BaTi_{0.7}Zr_{0.3}O₃ relaxor ferroelectrics. *Results Phys.* **2019**, *15*, 102799. [[CrossRef](#)]



© 2020 by the authors. Licensee MDPI, Basel, Switzerland. This article is an open access article distributed under the terms and conditions of the Creative Commons Attribution (CC BY) license (<http://creativecommons.org/licenses/by/4.0/>).